Eur. J. Mineral.
2013, **25**, 145–153
Published online December 2012

# Origin of twist in 'gwindel' quartz crystals from the Alps: a transmission electron microscopy study

PATRICK CORDIER[1,*] and FLORIAN HEIDELBACH[2,3]

[1] Unité Matériaux et Transformations, Université Lille 1, UMR CNRS 8207, 59655 Villeneuve d'Ascq Cedex, France
*Corresponding author, e-mail: Patrick.Cordier@univ-lille1.fr
[2] Bayerisches Geoinstitut, Universität Bayreuth, Germany
[3] Present address: Bruker Nano GmbH, Berlin, Germany

**Abstract:** Two twisted quartz crystals (gwindels) from the Alps were studied by transmission electron microscopy and large-angle convergent-beam electron diffraction (LACBED) to elucidate the twist mechanism. We found that torsion results from a distribution of straight screw geometrically necessary $\boldsymbol{b} = \frac{1}{3}\langle 2\bar{1}\bar{1}0\rangle$ dislocations with a dislocation density of the order of $10^{10}$ m$^{-2}$. This dislocation microstructure induces an Eshelby twist which can account for the observed twist of a few degrees per centimetre. This microstructure suggests that twisted gwindel quartz forms by the spiral growth mechanism which enables crystal growth under small driving forces.

**Key-words:** twisted quartz, gwindel, geometrically necessary dislocations, screw dislocations, transmission electron microscopy, crystal growth.

## 1. Introduction

Controlling and designing the morphology of crystals is a very active challenge in nanotechnology. Recent reports on dislocation-driven nanowire growth (Bierman *et al.*, 2008; Morin & Jin, 2010) have rejuvenated interest in the control of large twists in crystals. This phenomenon, although rare is observed in Nature in some minerals. In particular, quartz crystals from the Alps called gwindel[1] exhibit a macroscopic twist of a few degrees per centimetre. This phenomenon has been known and described for a long time but its physical origin remains to be identified.

The first description of twisted quartz is probably due to Weiss (1836), who describes crystals elongated along one of the *a*-axes and with *c*-axis rotating around this *a*-axis. Tschermak (1894) has described several twisted quartz and has proposed a classification based on the morphology, which is still in use. He distinguishes: (1) *''open'' specimens*, showing individual quartz crystals with their rhombohedral faces helically rotating around a common *a*-axis; (2) *''half-closed'' specimens*, with individual quartz crystals developing on one side only and (3) *''closed'' specimens*: rectangular-shaped crystals with smooth and continuous edges exhibiting twist around the long *a*-axis. Tschermak (1894) has also proposed that twist may be related to some twinning. This suggestion was abandoned since geometrical measurements showed no systematic relationships between faces. The first physical characterization was performed in 1935 by Nowacki. Using X-ray diffraction he showed that twisted quartz crystals exhibit ''normal'' quartz diffraction patterns. These patterns showed some anomalies, however, since some diffraction spots were elongated. Laemmlein (1937) studied a large body of crystals from subarctic Urals (55 crystals) and Switzerland (26 crystals) and pointed out that twisting occurs very early in the growth process, before the crystal breaks into domains (the so-called macromosaicism) and before individual prisms form. This observation has been further confirmed by Poty (1967). On the contrary, Friedlaender (1951) has mostly studied the late stage of growth which leads to the formation of individually distinct crystals. The observed angle of twist is almost always between 1° and 5° per centimetre (Frondel, 1962; Rykart, 1989) although Stalder *et al.* (1998) report 13° per centimetre as the upper limit of the normal range.

We propose here a study based on transmission electron microscopy to elucidate the origin of such large twist angles in quartz. Following the suggestion of Poty (1967), we concentrate on the central region of twisted crystals supposed to represent the early stage of twist formation.

## 2. Samples

Two gwindel quartz samples have been investigated in the course of this study. Sample B8789 was provided to us by Dr. Gérard Dolino and comes from the Natural History Museum

[1]The name ''Gwindel'', commonly used in Switzerland, derived from the German ''gewunden'', which means helicoidal, twisted

DOI: 10.1127/0935-1221/2013/0025-2271
0935-1221/13/0025-2271 $ 4.05

Bern, Switzerland. In this sample, the seed, *ca.* $1 \times 2 \times 6\ cm^3$ is twisted (a few degrees per centimetre) around the long dimension OX (corresponding to an *a*-axis). It is surrounded by an envelope of domains elongated along OZ (corresponding to the *c*-axis), showing macromosaicism and with relative misorientations of 1–3°. The TEM samples were prepared from a plate ($0.5 \times 3 \times 1$ cm) perpendicular to OX and cut from the central part of this crystal.

The second sample (BP-10-1) was provided to us by Prof. Bernard Poty and was found in the Mont Blanc Massif, French Alps. It is a right-handed twisted quartz representing an early stage of torsion. The external part shows macromosaicism however.

## 3. Microstructural investigation

### 3.1. Electron backscatter diffraction

Electron backscatter diffraction (EBSD) was performed in Bayreuth on a Leo (now Zeiss) Gemini 1530 scanning electron microscope (SEM) with a Schottky emitter, equipped with a detector for forward scattered electrons (FSE) for orientation contrast imaging and a camera for the detection of patterns, both from Oxford Instruments. Figure 1 shows a map recorded on a basal (0001) thin section (*ca.* 30 µm thick) in the twisted region. One

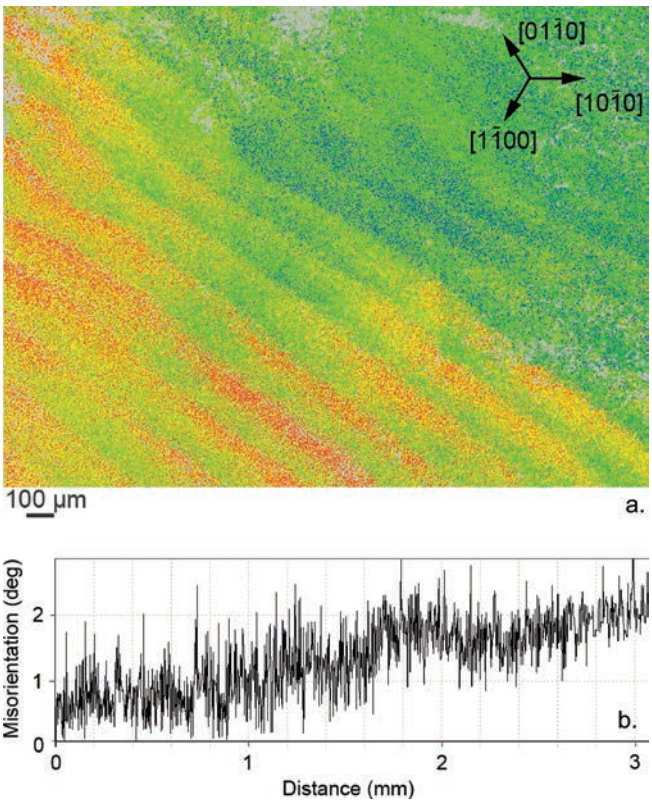


Fig. 1. Sample B8789–twisted region. (a) EBSD map recorded on a basal thin (*ca.* 30 µm) section. (b) Misorientation profile recorded on a line joining the lower left to the upper right-hand corner of the map.

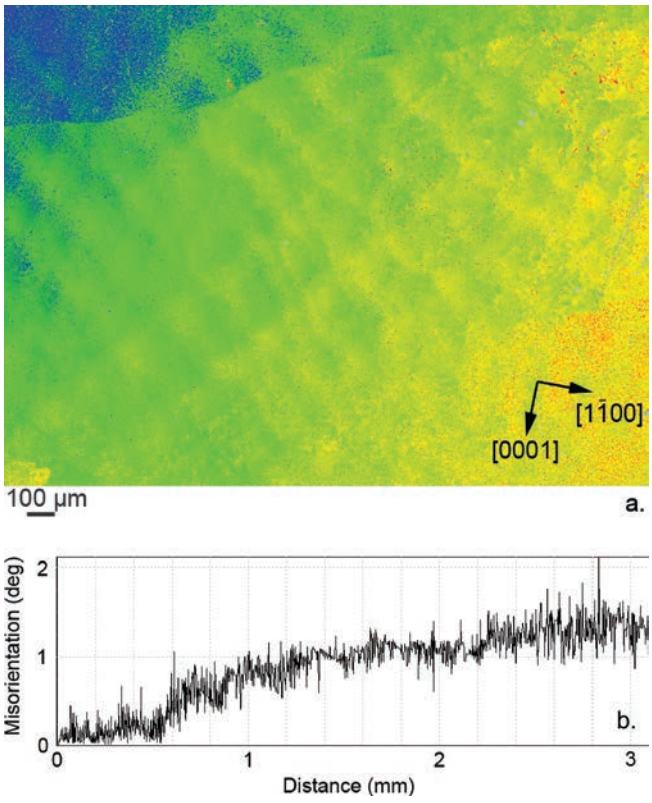


Fig. 2. Sample B8789–twisted region. (a) EBSD map recorded on a prismatic (11$\bar{2}$0) thin (*ca.* 30 µm) section. (b) Misorientation profile recorded on a line joining the lower left to the upper right-hand corner of the map.

observes a wavy structure with very small misorientations (basically within the noise) from point to point (1.5 µm step size) which develops perpendicular to $<1\bar{1}00>$. Overall a misorientation of about 2° accumulates over the measured length (3 mm). Figure 2 shows another view (also on a 30 µm thick thin section) on a section parallel to a prismatic plane (11$\bar{2}$0). A periodic structure with a wavelength compatible with the one of Fig. 1 is observed. Altogether, these observations suggest that these periodic structures develop on some $\{10\bar{1}1\}$ planes.

### 3.2. Transmission electron microscopy

#### *3.2.1. Internal twisted region*

A thin foil was extracted from the section mapped in Fig. 1 and was ion-thinned until electron transparency. This specimen contains numerous microcracks (Fig. 3a) which exhibit no preferred orientations. It contains also a few long (several tens of micrometres within the thin foil) straight defects (Fig. 3a and b). Although these defects look like dislocations at low magnification, their contrast (in bright or dark-field or as a function of the Bragg error) is not conventional. Indeed, Fig. 3 shows discontinuous features along the line. To characterize these defects, we have used large-angle convergent-beam electron diffraction (LACBED, Tanaka *et al.*, 1980). This technique which uses a defocused beam

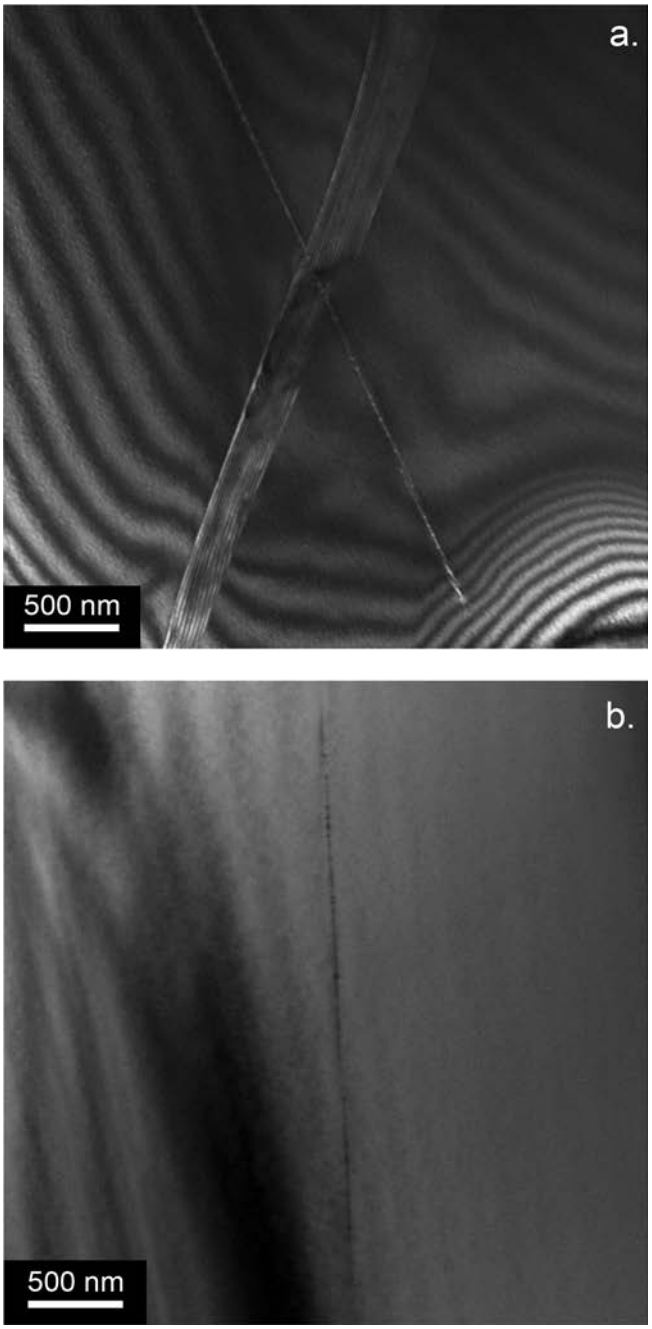


Fig. 3. Sample B8789–TEM observation on a thin foil extracted from the thin section mapped on Fig. 1. (a) This sample contains a lot of microcracks. One of them is crossed here by a long straight dislocation. Weak-beam dark-field micrograph with g: $10\bar{1}1$. (b) Another long straight dislocation. Note the contrast in the core. Bright-field micrograph with g: $10\bar{1}1$.

allows diffraction mapping superimposed to an image of the sample and has proved to be very efficient in characterizing crystal defects (Morniroli, 2002). The characterization has been undertaken close to the $[\bar{1}2\bar{1}6]$ zone axis (Fig. 4a and b). When the dislocation line is brought close to the zone axis and crosses Bragg lines, these are distorted by the strain field of the dislocation (Fig. 4c). The effect observed on the Bragg lines (local rotation of the line and splitting into fringes) is typical of the one of a dislocation. This confirms the nature (dislocations) of the linear defects observed in this specimen despite their fuzzy contrasts. Cherns & Preston (1986) have shown that the effect of dislocations on LACBED patterns can be interpreted very easily since the interfringe number $n$ is simply the dot product $\boldsymbol{g}.\boldsymbol{b}$ where $\boldsymbol{g}$ is the reciprocal lattice vector representing diffracting planes and $\boldsymbol{b}$ is the dislocation Burgers vector. Figure 4d shows an enlargement of this experiment where some Bragg lines have been indexed. Knowing the direction of the excitation vector (from comparison with kinematic simulations performed with the software ''Electron Diffraction'' from J.P. Morniroli) allows one to determine the sign of the $\boldsymbol{g}_i.\boldsymbol{b} = n_i$ product by applying the Cherns & Preston (1986) rules. From the effects shown in Fig. 4d, one can write a linear system[2] the solution of which is the Burgers vector $b = [u_b\ v_b\ w_b]$:

$$\begin{cases} -3u_b - 3v_b + 2w_b = -3 \\ -6u_b + v_b = -6 \\ 2u_b - 2v_b + w_b = 2 \\ 6u_b - 4v_b + 2w_b = 6 \\ -3u_b + 4v_b - 2w_b = -3 \end{cases}$$

The unique solution of this system is $b = [100] = \frac{1}{3}\left[2\overline{1}\overline{1}0\right]$.

In fact, more effects have been observed from this dislocation, they are presented in Table 1. They are all consistent with the same Burgers vector. To characterize the line direction of the dislocation, the specimen has been tilted back to the [0001] zone axis (*i.e.* with the beam direction parallel to the c-axis) which corresponds to the mean orientation of the thin foil (Fig. 5). Along this orientation, one can see that the dislocation line is parallel to the $(01\bar{1}0)$ Bragg line (see Morniroli & Gaillot, 2000 for trace analysis in LACBED). Its line direction is thus contained in both the basal (0001) plane (thin-foil plane) and in the $(01\bar{1}0)$ plane. Its line direction is thus $L = [2\bar{1}\bar{1}0]$ showing that the dislocation is of pure screw character.

Figure 6 shows a TEM observation from another foil from specimen BP-10-1 cut perpendicular to the twist axis. Consistent with previous observations, one observes numerous contrasts which are compatible with dislocations viewed end-on. To further demonstrate that they indeed correspond to dislocations, we have tilted the specimen to show the dislocation lines. However, this cannot be done with one of the $10\bar{1}1$ diffraction vector which, in quartz, provide the best contrast (Table 2 shows the intensity and extinction distances for some diffraction vectors in quartz). To provide a contrast of sufficient quality to identify the dislocation lines, we have selected the second best diffraction plane $\{\bar{1}2\bar{1}2\}$ that is accessible to tilt in our specimen. The corresponding image is shown on Fig. 7 where one can see that the contrasts seen in Fig. 6 do correspond to

[2]In quartz which is trigonal, planes and direction can be described within two settings using either three (Miller) or four (Miller-Bravais) indices. Both will be used here since Miller indices are more adapted when calculations are made and Miller-Bravais indices are more adapted to describe the results and emphasize the symmetries of the hexagonal lattice. See electronic Appendix at GSW site for the description of Miller-Bravais indices and relationships between the two descriptions (www.eurjmin.geoscienceworld.org).

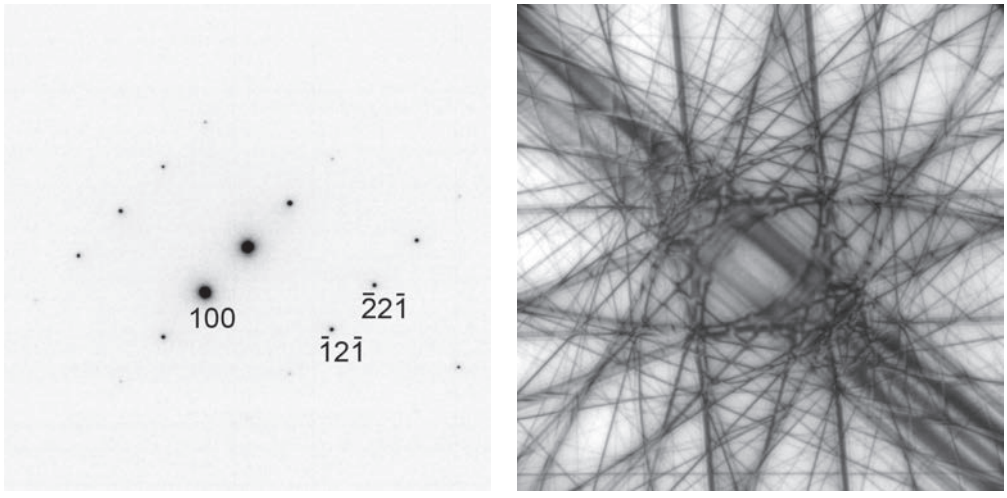


a. b.

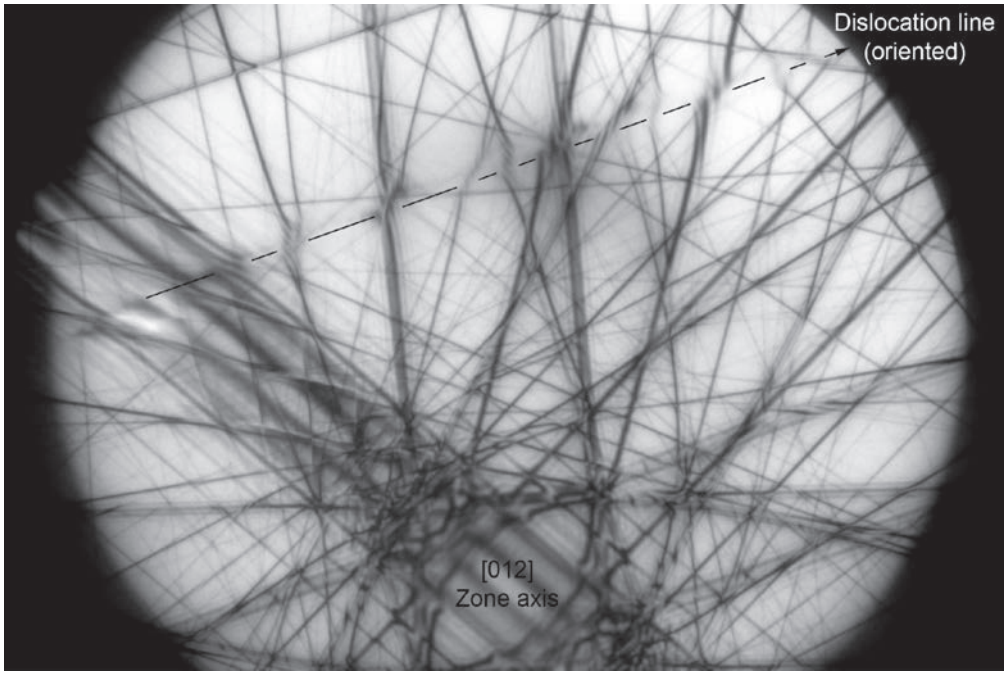


c.

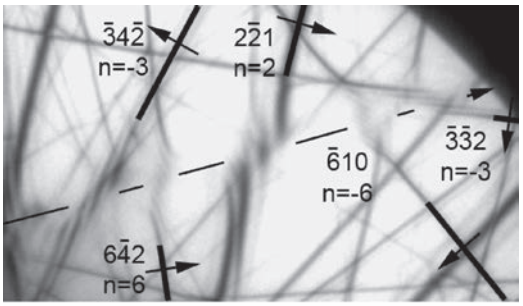


d.

Fig. 4. LACBED characterization of the Burgers vector $\boldsymbol{b}$ of one of these long straight dislocations in sample B8789. (a) The characterization is made close to the $[012] = \frac{1}{3}\left[\bar{1}2\bar{1}6\right]$ zone axis seen here in selected area diffraction and in (b) in LACBED. (c) A long dislocation (arrow) crosses several Bragg lines close to the $[012] = \frac{1}{3}\left[\bar{1}2\bar{1}6\right]$ zone axis. The dislocation is detected through the characteristic effect (rotation and splitting) on the Bragg lines crossed. (d) An enlargement of (c) with some Bragg lines indexed. The arrows provide the orientation of the deviation parameter $s$. The sign of the $\boldsymbol{g}.\boldsymbol{b} = n$ products are found according to the Cherns & Preston rules. The Burgers vector is $b = [100] = \frac{1}{3}\left[2\bar{1}\bar{1}0\right]$.

Table 1. Summary of all effects independently observed in LACBED for the characterization of the Burgers vector of the dislocation shown in Fig. 3 (most of them can be seen on Fig. 4). They are all consistent with $\boldsymbol{b} = [100] = \frac{1}{3}\left[2\bar{1}\bar{1}0\right]$, although the three first are sufficient for a determination.

| Bragg line | $n$ (observed) | $\boldsymbol{g}.\boldsymbol{b}$ product for $b = [100]$ |
|---|---|---|
| $\bar{3}\,\bar{3}\,2$ | −3 | −3 |
| $\bar{6}\,1\,0$ | −6 | −6 |
| $2\,\bar{2}\,1$ | 2 | 2 |
| $4\,\bar{4}\,2$ | 4 | 4 |
| $6\,\bar{4}\,2$ | 6 | 6 |
| $\bar{3}\,4\,\bar{2}$ | −3 | −3 |
| $4\,\bar{2}\,1$ | 4 | 4 |
| $\bar{4}\,4\,\bar{2}$ | −4 | −4 |
| $\bar{4}\,2\,\bar{1}$ | −4 | −4 |
| $2\,0\,0$ | 2 | 2 |
| $1\,\bar{2}\,1$ | 1 | 1 |

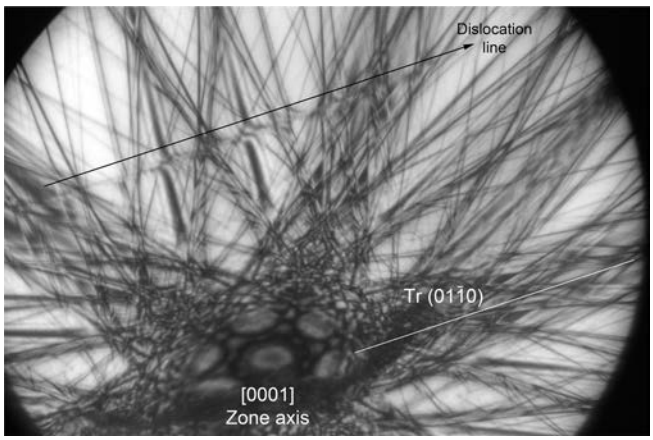


Fig. 5. LACBED characterization of the line direction vector $L$ of the dislocation from Fig. 4. The specimen is oriented along the [0001] zone axis. Since this corresponds to the untilted position of the specimen in the microscope, the mean orientation of the thin foil (which contains the long dislocation line) is parallel to the basal plane (0001). When the dislocation line is placed on the zone axis, it is shown to be parallel to the (010) Bragg line (here the dislocation is moved slightly aside for a better visibility. It is highlighted by an arrow placed just above the characteristic effects on the Bragg line, which allows one to locate the dislocation line). Its line is thus contained in both the (0001) plane (thin foil plane) and in the (01$\bar{1}$0) plane. Its line direction vector is thus $L = \left[2\bar{1}\bar{1}0\right]$. The dislocation is of pure screw character.

dislocations parallel to the *a*-axis. This foil orientation is more adapted to evaluate the dislocation density than the previous one. Counting the number of dislocations per unit area leads to a dislocation density of *ca.* $10^{10}$ m$^{-2}$, corresponding to a mean distance between dislocations of the order of 10 μm.

### *3.2.2. Outer macromosaic region*

A few observations were made in the outer regions of the specimen which show macromosaicism. Figure 8 shows

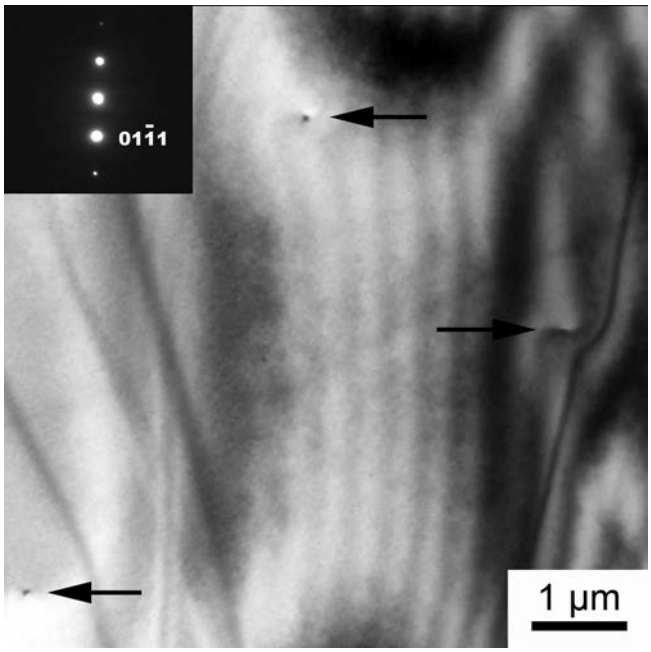


Fig. 6. Sample BP-10-1, thin section perpendicular to the twist axis – Dark field micrograph with g: 01$\bar{1}$1. Numerous contrasts are observed which are consistent with dislocations seen end-on (arrowed).

Table 2. Extinction distance and intensity for the most efficient reflection planes in α-quartz sorted in order of decreasing intensity (calculations made at 300 kV with the software ''Electron Diffraction'' from J.P. Morniroli).

| Reflection $\{hkil\}$ | $d_{hkl}$ (Å) | Extinction distance (Å) | Intensity |
|---|---|---|---|
| $\{0\,1\,\bar{1}\,1\}$ | 3.3436 | 960 | 353 |
| $\{1\,1\,\bar{2}\,2\}$ | 1.8180 | 2027 | 79 |
| $\{0\,3\,\bar{3}\,1\}$ | 1.3721 | 2082 | 75 |
| $\{0\,1\,\bar{1}\,0\}$ | 4.2556 | 2164 | 70 |
| $\{0\,1\,\bar{1}\,2\}$ | 2.2814 | 2446 | 54 |
| $\{0\,2\,\bar{2}\,2\}$ | 1.6718 | 2455 | 54 |
| $\{1\,1\,\bar{2}\,0\}$ | 2.4570 | 2474 | 53 |

that at the TEM scale as at the optical scale, the boundaries associated with macromosaicism exhibit no particular orientations. Although some rare dislocations have been seen (not the specific straight screws reported above), we could not correlate any microstructure or feature with the boundaries. Electron diffraction (Fig. 8c and d) shows that, across the boundary, the crystal is slightly misoriented (1.2°) in agreement with optical observations.

## 4. Discussion

The two crystals investigated here yield consistent observations. The central twisted regions of the crystals

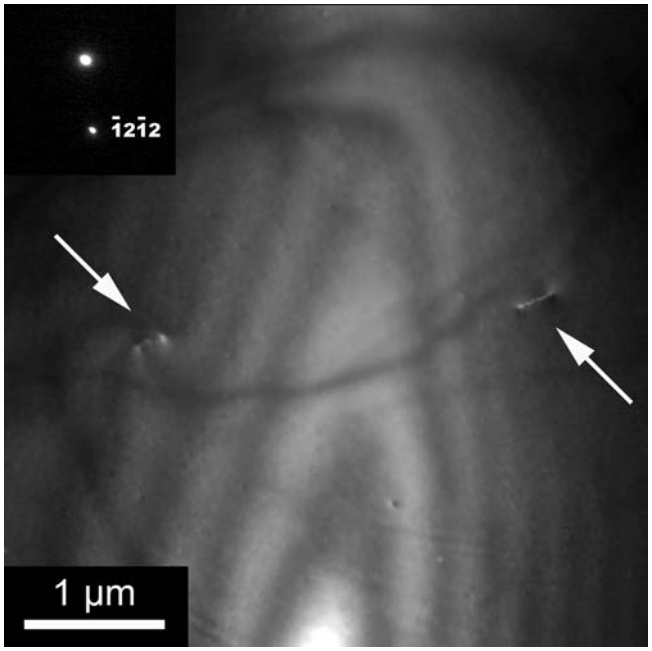


Fig. 7. Sample BP-10-1, same thin section as Fig. 6. Weak-beam dark-field micrograph with g: $\bar{1}2\bar{1}2$. The specimen is tilted at *ca.* 25° compared to Fig. 6. The dislocations appear as short segments.

investigated are characterized by the presence of long straight screw $\boldsymbol{b} = \frac{1}{3}\langle 2\bar{1}\bar{1}0\rangle$ dislocations. These dislocations exhibit a particular, ambiguous, contrast. However, LACBED was able (i) to map the strain field around the defects and to show a behaviour characteristic of a dislocation and (ii) to characterize the Burgers vector. These defects are thus consistent with growth dislocations. It is difficult to decide whether the observed contrast is due to etching along the dislocation line (leading to a partially hollow core) or to some foreign materials (impurities, nanoparticles) within the core. However, microanalysis in the STEM mode could not reveal any convincing evidence for impurities in the dislocation cores.

The mean dislocation density has been measured to be of *ca.* $10^{10}$ m$^{-2}$. However, EBSD measurements suggest that screw dislocations are not completely randomly distributed since some patterning is shown. The observed wavelength associated with these patterns is between 100 and 200 μm. This order of magnitude is not adapted for gaining more information at the TEM scale on this patterning.

It is a classical result of Eshelby (1953) that the presence of a screw dislocation (Burgers vector $\boldsymbol{b}$) along the axis of a circular cylinder (radius $R$) is responsible for a uniform twist α (the so-called Eshelby twist) equal (in radians per unit length) to:

$$\alpha = \frac{\boldsymbol{b}}{\pi R^2} \tag{1}$$

This result has been extended to rods with any cross section (Eshelby, 1958) by multiplying the previous expression by a constant $k$ (close to 1!) characteristic of the cross-sectional shape. The $1/R^2$ dependence of the Eshelby twist has led some to look for experimental evidence of it on micrometre-sized whiskers (*e.g.* Sears, 1959). Evidence for the Eshelby twist is commonly observed in the TEM since it is responsible for local displacements observable in high-resolution transmission electron microscopy close to the dislocation core where it meets free surfaces (Cosgriff *et al.*, 2010; Gröger *et al.*, 2011). Nanotechnologies provide new evidence for Eshelby twists: for instance, Bierman *et al.* (2008) show a spectacular example of pine tree like nanowires with helically rotating epitaxial branch nanowires.

The displacement field of straight screw $b = \frac{1}{3}\langle 2\bar{1}\bar{1}0\rangle$ dislocations is responsible for an Eshelby twist which is geometrically compatible with the torsion observed at the macroscopic scale in twisted gwindel quartz with a twist axis along an *a*-axis inducing rotation of the c-axis. However, quantitative aspects are difficult to assess since the case described by Eshelby considers only one dislocation in a cylinder. Recently, Weinberger & Cai (2010) have shown that, even in the case of small systems, a distribution of several screw dislocations aligned with the cylinder axis can result in a stable configuration and produce twist. At a more macroscopic level, one can refer to strain gradient plasticity theories which have been developed to describe non-homogeneous deformation. To account for non-homogeneous deformation, Ashby (1970) has introduced the concept of geometrically necessary dislocations (GND) which are distinguished from statistically stored dislocations (which develop in homogeneous deformation). Torsion represents a typical case of non-homogeneous deformation which has been described by Fleck *et al.* (1994). They have shown that in a circular wire deformed in torsion (macroscopic twist angle $\alpha^M$), the strain gradient is produced by a density $\rho$ (in m$^{-2}$) of GND (screw dislocations of Burgers vectors $\boldsymbol{b}$) of the order of:

$$\rho = \frac{\alpha^M}{b} \tag{2}$$

Introducing $\rho = 10^{10}$ m$^{-2}$ and $\boldsymbol{b} = 4.912$ Å in (2), one finds $\alpha^M = 4.9$ radians/m, i.e. 8.8 degrees per centimetre. The dislocation density observed is thus perfectly able to produce the strain (twist) observed, providing further validation for our observations.

Altogether, our investigation leads us to the conclusion that twist in quartz crystals result from a self-organized distribution of straight screw $b = \frac{1}{3}\langle 2\bar{1}\bar{1}0\rangle$ geometrically necessary dislocations with a density $\rho \approx 10^{10}$ m$^{-2}$, which formed during growth. It is interesting to note that this explains the observation reported by Laemmlein (1937) that chemical etching by hydrofluoric acid of *closed* crystals leads to the formation of long and narrow etched channels. This technique has been used to visualize dislocations structures in quartz (Hanyu, 1964) or in garnet (Carstens, 1969) within a polished thin section.

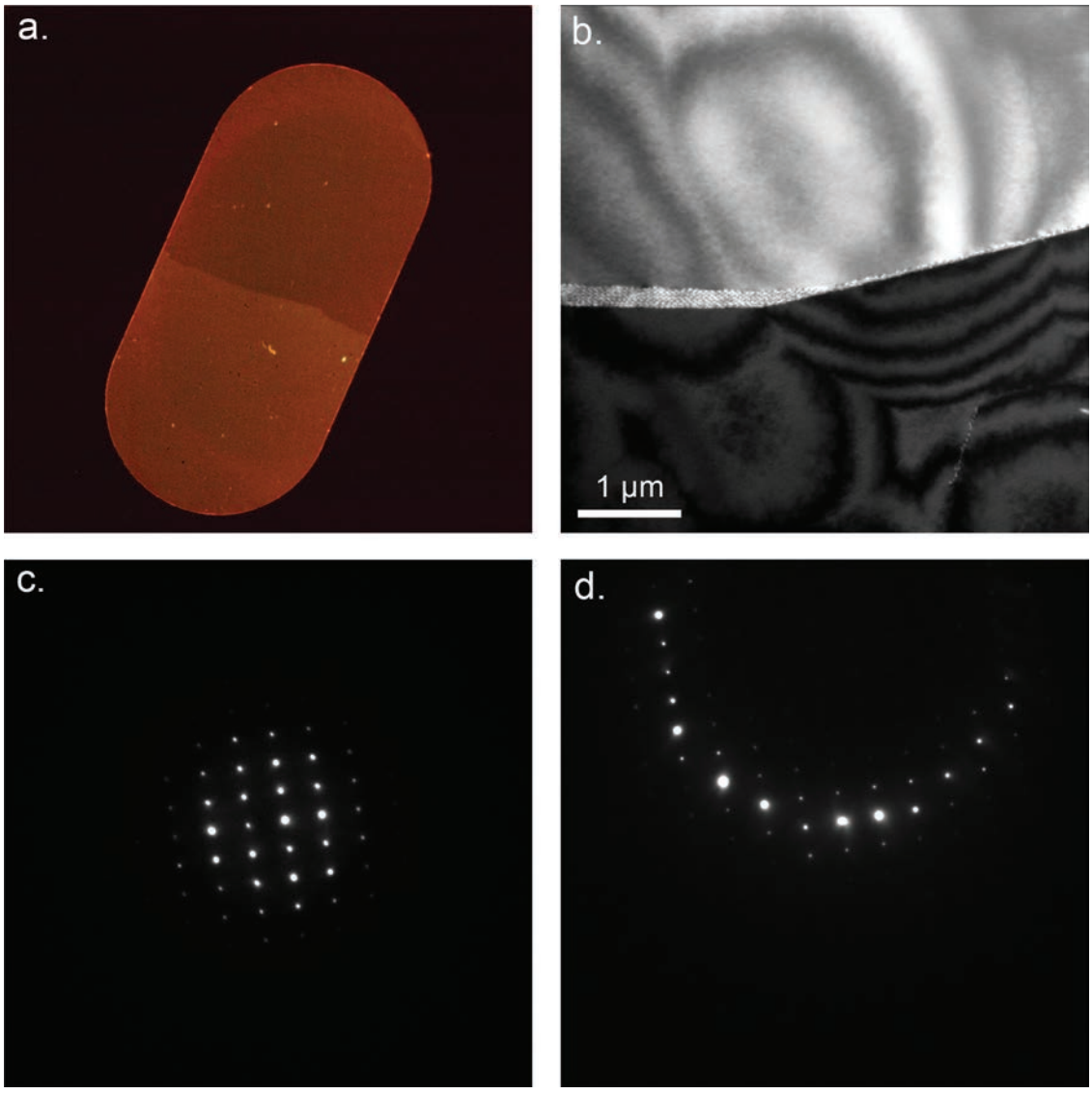


Fig. 8. Sample BP-10-1, outer region exhibiting macromosaicism. (a) Optical micrograph (crossed nicols) of the specimen before ion thinning (mounted on a copper grid with a 2 mm × 1 mm hole which gives the scale). A boundary runs in the middle of the TEM specimen and ion thinning has been adjusted so as to have the boundary in electron-transparent areas. (b) same boundary seen at the TEM. Dark-field with g:$10\bar{1}1$. (c) Selected-area diffraction pattern (SAED) on one side of the boundary. The specimen is orientated in such a way that this side is along the $[2\bar{1}\bar{1}0]$ zone axis. (d) Without tilting the specimen, a SAED pattern is recorded from the other side of the boundary. The misorientation is 1.2°.

This density of geometrically necessary dislocations is a source of internal stresses as shown by the numerous microcracks observed. We cannot know whether these microcracks were present in the bulk material or whether they were induced during sample preparation. In any case, they reveal the presence of substantial internal stresses and strain energy. A screw dislocation (core radius $r_c$) contained in a cylinder (radius $R$) is responsible for a strain energy $E$ per unit length:

$$E = \frac{\mu b^2}{4\pi} \ln\left(\frac{R}{r_c}\right) \tag{3}$$

As growth proceeds, the crystal stores an increasing strain energy which eventually exceeds the critical energy necessary for creating grain boundaries. To prevent this strain energy from further increasing, the crystal breaks into slightly misoriented blocks (the so-called macromosaicism) which relax internal stresses and allow further growth.

As to the reasons for such a peculiar growth process, we can only put forward educated guesses. Twisted gwindel quartz exhibit morphologies that are clearly distinctive from usual natural quartz. Besides being twisted, they are elongated along an *a*-axis instead of the *c*-axis for normal prismatic quartz crystals (Poty, 1967; Ihinger & Zink, 2000). The growth of twisted quartz clearly occurs under conditions that are unfavorable for normal growth of quartz. This is likely because the driving force (supersaturation) was too

low (although we cannot disregard the possibility that the growth surface was poisoned by some surfactants: Gyulai, 1963; Teng *et al.*, 1998). Indeed, twisted gwindel quartz seems to grow in a temperature window between 350 and 450°C, whereas below 300°C gwindels are never found (Poty, personal communication). Frank (1949, 1952) first proposed that screw dislocations could provide an efficient mechanism to enhance crystal growth at small driving forces. This gave rise to the classical BCF theory on spiral growth named after the initials of the authors Burton, Cabrera and Frank (1951). Experimental support for this model was rapidly provided by Griffin (1950) who observed monomolecular layers on the $(10\bar{1}0)$ face of a beryl crystal and by Verma & Amelinckx (1951) who showed a growth front spiraling outward around a central point on the growth surface of carborundum (SiC). The measurements confirmed the height of the growing layer as a single unit cell. Later, Gyulai (1963) gave an elegant demonstration of this principle. In the presence of polyvinyl alcohol, crystal growth of sodium chloride is inhibited since slowly growing faces are poisoned by adsorbed alcohol. After having been twisted to introduce screw dislocations, a small crystal of sodium chloride showed rapid growth of needles forming uniform helicoids. Indeed, a crystal containing a screw dislocation can grow easily because an atomic ledge is always present to accept adatoms and promote crystal growth. The spiral growth model has now been shown to operate in a large variety of compounds (Yip & Ward, 1996; Paloczi *et al.*, 1998; Teng *et al.*, 1998; Cuppen *et al.*, 2004; Ranguelov *et al.*, 2006). Following the pioneering work of Gyulai (1963), dislocations are used to ''engineer'' growth of 1D architectures suited for specific purposes. Morin & Jin (2010) have intentionally used screw dislocations in defect-rich gallium nitride (GaN) thin films to propagate dislocation-driven growth of zinc oxide (ZnO) nanowires.

In the present case, we have tried to verify whether the contrast observed in the dislocation cores would be related to impurities related to crystal growth poisoning but we could not find any convincing chemical evidence. Whatever has affected ''normal'' growth of these crystals, it is clear that the presence of screw dislocations has provided an alternative mechanism for crystal growth leading to this particular morphology. Twisted gwindel quartz represents here an original case since the collective contribution of a large number of dislocations with the same sign yields large values of Eshelby twists, visible at the macroscopic scale. In his original paper, Frank (1949) has considered the possibility that several screw dislocations could arrange and produce *visible* growth terraces. The collaborative effect of several screw dislocations of the same sign was also discussed by Burton *et al.* (1951). More quantitatively, Smereka (2000) has shown that the asymptotic growth rate for co-rotating spirals (produced by screw dislocations of the same sign) is greater than that for a single spiral and that the growth rate increases as the distance between the screw dislocations is decreased.

The microstructure observed in twisted gwindel quartz appears thus to be characteristic of growth under small driving force enhanced by the spiral growth mechanism (Sunegawa, 1999).

## 5. Conclusion

We show here that the twist of a few degrees per centimetre observed in two natural twisted gwindel quartz crystals from the Alps is due to geometrically necessary screw $\boldsymbol{b} = \frac{1}{3}\langle 2\bar{1}\bar{1}0\rangle$ dislocations. This distribution, characterized by a dislocation density of *ca.* $10^{10}$ m$^{-2}$ is self-organized at the sub-millimetre scale with a wavelength of *ca.* 100–200 μm. This is the first report of an Eshelby twist with an amplitude detected at the macroscopic scale. This is due to the collective contribution of a large number of dislocations, demonstrating that twisting crystals is not only possible at the microscopic scale.

We propose that this microstructure achieves an enhanced crystal growth rate in response to unfavorable growth conditions, like low driving force or passivated (poisoned) growth surfaces.

## Note added in proof

It must be noted that the hypothesis that twisting in quartz derives from screw dislocations was originally proposed by Clifford Frondel in1978 in a study on twisted quartz fibers and single crystals. The authors were unaware of this work during preparation of the present publication.

**Acknowledgements:** One of us (PC) thanks G. Dolino and B. Poty for having drawn his attention on the ''twisted quartz'' issue and for constructive comments on the manuscript. The crystals investigated in this study have been provided originally by Jean-Marie Buzzarello and Xavier Jeambrun (who discovered the vein containing crystal (BP-10-1) in the Mont-Blanc massif) and Beda Hofmann (Natural History Museum Bern) to whom we are grateful. We thank Dr Edwin Gnos (Museum of Natural History, Geneva) for fruitful discussions on twisted crystals and two anonymous reviewers for useful comments on the manuscript.

## References

Ashby, M.F. (1970): The deformation of plastically non-homogeneous materials. *Phil. Mag.*, **21**, 399–424.

Bierman, M.J., Lau, Y.K.A., Kvit, A.V., Schmitt, A.L., Jin, S. (2008): Dislocation-driven nanowire growth and Eshelby twist. *Science*, **320**, 1060–1063.

Burton, W.K., Cabrera, N., Frank, F.C. (1951): The growth of crystals and the equilibrium structure of their surfaces. *Phil. Trans. R. Soc. Lond. A*, **243**, 299–358.

Carstens, H. (1969): Dislocation structures in pyropes from Norwegian and Czech garnet peridotites. *Contrib. Mineral. Petrol*, **24**, 348–353.

Cherns, D. & Preston, A.R. (1986): CBED studies of crystal defects. *in* ''Proceedings ICEM-11'', Kyoto, 721–722.

Cosgriff, E.C., Nellist, P.D., Hirsh, P.B., Zhou, Z., Cockayne, D.J.H.. (2010): ADF STEM imaging of screw dislocations viewed end-on. *Phil. Mag*., **90**, 4361–4375.

Cuppen, H.M., Graswinckel, W.S., Meekes, H. (2004): Screw dislocations on polycenes: a requirement for crystallization. *Cryst. Growth Design*, **4**, 1351–1357.

Eshelby, J.D. (1953): Screw dislocations in thin rods. *J. Appl. Phys*., **24**, 176–179.

— (1958): The twist in a crystal whisker containing a dislocation. *Phil. Mag*., **3**, 440–447.

Fleck, N.A., Muller, G.M., Ashby, M.F., Hutchinson, J.W. (1994): Strain gradient plasticity: theory and experiment. *Acta Metall. Mater*., **42**, 475–487.

Frank, F.C. (1949): The influence of dislocations on crystal growth. *Discuss. Faraday Soc*., **5**, 48–54.

Frank, F.C. (1952): Crystal growth and dislocations. *Adv. Phys*., **1**, 91–109.

Friedlaender, C. (1951): Untersuchung über die Eignung alpiner Quarze für piezoelektrische Zwecke. *Beitr. Geol. Schweiz, Geotech. Ser*, **29**, 1–98.

Frondel, C. (1962): The system of mineralogy of Dana. III. Silica Minerals. John Wiley, New York and London, 334 p.

Griffin, L.J. (1950): Observation of unimolecular growth steps on crystal surfaces. *Phil. Mag*., **41**, 196–199.

Gröger, R., Dudeck, K.J., Nellist, P.D., Vitek, V., Hirsh, P.B., Cockayne, D.J.H. (2011): Effect of Eshelby twist on core structure of screw dislocations in molybdenum: atomic structure and electron microscope image simulations. *Phil. Mag*., **19**, 2364–2381.

Gyulai, Z. (1963): Das Weiterwachsen von plastisch deformierten NaCl-Kristallen. *Z. Physik*., **176**, 370–379.

Hanyu, T. (1964): Dislocation etch tunnels in quartz crystals. *J. Phys. Soc. Jpn*, **19**, 1489.

Ihinger, P.D. & Zink, S.I. (2000): Determination of relative growth rates of natural quartz crystals. *Nature*, **404**, 865–869.

Laemmlein, G.G. (1937): Observations on the twisted quartz (in Russian). *Izvestia Acad. Nauk SSSR*, 937–964.

Morin, S.A. & Jin, S. (2010): Screw dislocation-driven epitaxial solution growth of ZnO nanowires seeded by dislocations in GaN substrates. *Nano. Lett*., **10**, 3459–3463.

Morniroli, J.P. (2002): Large-angle convergent-beam electron diffraction (LACBED). Application to crystal defects. Monograph of the French Society of Microscopies, Paris, 432 p.

Morniroli, J.P. & Gaillot, F. (2000): Trace analyses from LACBED patterns. *Ultramicroscopy*, **83**, 227–243.

Nowacki, W. (1935): Gewundene Quarze. *Schweiz. Mineral. Petrog. Mitt*, **15**, 408–409.

Paloczi, G.T., Smith, B.L., Hansma, P.K., Walters, D.A., Wendman, M.A.. (1998): Rapid imaging of calcite crystal growth using atomic force microscopy with small cantilevers. *J. Appl. Phys*., **73**, 1658–1660.

Poty, B. (1967): La croissance des cristaux de quartz dans les filons sur l'exemple du filon de La Gardette (Bourg d'Oisans) et des filons du massif du Mont-Blanc. Thèse de Doctorat ès Sciences Naturelles de l'Université de Nancy, 162 p.

Ranguelov, B., Metois, J.J., Muller, P. (2006): Spirals on Si(111) at sublimation and growth: REM and LODREM observations. *Surf. Sci*., **600**, 4848–4854.

Rykart, R. (1989): Quartz-Monographie. Ott-Verlag, Thun, 462 p.

Sears, G.W. (1959): Twist in lithium fluoride whiskers. *J. Chem. Phys*., **31**, 53–54.

Smereka, P. (2000): Spiral crystal growth. *Phys. D*, **138**, 282–301.

Stalder, H.A., Wagner, A., Graeser, S., Stuker, P. (1998): Mineralienlexikon der Schweiz. Verlag Wepf & Co., Basel, 579 p.

Sunagawa, I. (1999): Growth and morphology of crystals. *Forma*, **14**, 147–166.

Tanaka, M., Saito, R., Ueno, K., Harada, Y. (1980): Large-angle convergent-beam electron diffraction. *J. Electron. Microsc*., **29**, 408–412.

Teng, H.H., Dove, P.M., Orme, C.A., De Yoreo, J.J. (1998): Thermodynamics of calcite growth: baseline for understanding biomineral formation. *Science*, **282**, 724–727.

Tschermak, G. (1894): Über gewündene Bergkrystalle. *Denkschr., Akad. Wissen, Mat. Naturwiss.Cl. Wien*, **61**, 365–400.

Verma, A.R. & Amelinckx, S. (1951): Spiral growth on carborundum crystal faces. *Nature*, **167**, 939–940.

Weinberger, C.R. & Cai, W. (2010): Plasticity of metal wires in torsion: molecular dynamics and dislocation dynamics simulations. *J. Mech. Phys. Solids*, **58**, 1011–1025.

Weiss, S.C. (1836): Über rechts und links gewundene Bergkrystalle. *Abh. Königl. Akad. Wissen*, 187–205.

Yip, C.M. & Ward, M.D. (1996): Atomic force microscopy of insulin single crystal: direct visualization of molecules and crystal growth. *Biophys. J*., **71**, 1071–1078.

## Reference

Frondel, C. (1978): Characters of quartz fibers. Am. Mineral., **63**, 17–27.

*Received 26 September 2012*
*Modified version received 12 November 2012*
*Accepted 23 November 2012*